

Dalton Transactions

Accepted Manuscript

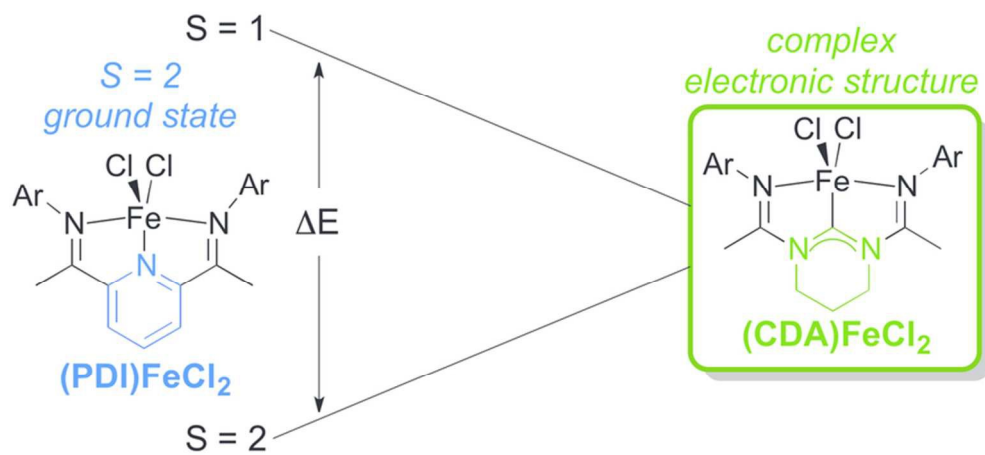


This is an *Accepted Manuscript*, which has been through the Royal Society of Chemistry peer review process and has been accepted for publication.

Accepted Manuscripts are published online shortly after acceptance, before technical editing, formatting and proof reading. Using this free service, authors can make their results available to the community, in citable form, before we publish the edited article. We will replace this *Accepted Manuscript* with the edited and formatted *Advance Article* as soon as it is available.

You can find more information about *Accepted Manuscripts* in the [Information for Authors](#).

Please note that technical editing may introduce minor changes to the text and/or graphics, which may alter content. The journal's standard [Terms & Conditions](#) and the [Ethical guidelines](#) still apply. In no event shall the Royal Society of Chemistry be held responsible for any errors or omissions in this *Accepted Manuscript* or any consequences arising from the use of any information it contains.



37x17mm (600 x 600 DPI)

COMMUNICATION

Spin Transitions in Bis(amidinato)-N-Heterocyclic Carbene Iron(II) and Iron(III) Complexes^a

Cite this: DOI: 10.1039/x0xx00000x

Jessica L. Drake,^b Hilan Z. Kaplan,^b Matthew J. T. Wilding,^c Bo Li,^b and Jeffery A. Byers^{b,*}Received 00th January 2012,
Accepted 00th January 2012

DOI: 10.1039/x0xx00000x

www.rsc.org/

In contrast to high spin pyridyl diimine iron(II) dichloride complexes, analogous bis(amidinato)-N-heterocyclic carbene iron(II) and iron(III) complexes demonstrate complex magnetic behaviour. In the solid state, they are best described as intermediate spin complexes at low temperatures that demonstrate gradual spin transitions beginning near or below room temperature. Treating the bis(amidinato)-N-heterocyclic carbene iron(II) complex with an aryl azide revealed enhanced reactivity compared to analogous complexes supported by pyridyl diimine ligands.

Since being discovered independently by Brookhart¹ and Gibson² as exceptionally active and selective ethylene polymerization catalysts, the chemistry of iron complexes bearing pyridyl diimine (PDI) ligands (e.g. **1**, Figure 1) has been of considerable interest to organometallic chemists. In addition to ethylene oligomerization,³ alkyne cyclotrimerization,⁴ atom transfer radical polymerization (ATRP),⁵ and lactide polymerization⁶ reactions that have been developed using iron(II) halide or alkoxide catalyst precursors, Chirik and co-workers have discovered that reduced PDI iron complexes lead to excellent catalysts for the hydrogenation,⁷ hydrosilylation,⁸ and hydroboration⁹ of olefins as well as the [2+2] cycloaddition of olefins and dienes.¹⁰

Inspired by the breadth of reactions catalysed by PDI iron complexes, our research group recently synthesized the first analogous pentacoordinate iron complex bearing a novel bis(amidinato)-N-heterocyclic carbene ligand (**2a**, Figure 1).^{11,12} Henceforth, we will refer to this ligand as carbenodiamidine, CDA. Noteworthy is the central trihydropyrimid-2-ylidene donor of CDA, which is a class of N-heterocyclic carbenes (NHCs) that had never been reported for iron complexes.¹³ We surmised that replacing the central pyridine of PDI ligands with a sterically similar, but electronically different NHC would significantly alter electronic structure and reactivity compared to **1**. Initial structural data and catalytic reactions supported this hypothesis. For example, deviations from typical metal–ligand bond distances were observed, including one of the shortest iron–carbene bond lengths observed to date (1.812(2) Å at 100 K).¹⁴ Additionally, the electron donating capabilities of CDA ligands were exploited for the generation of an

exceptionally active iron catalyst for lactide polymerization.¹⁵ Coupled with the need to better understand iron–NHC bonding, these findings prompted a more thorough inquiry into the electronic structure of iron complexes containing the CDA ligand. Moreover, the enhanced reactivity of CDA iron complexes compared to PDI iron complexes is illustrated by reactions between analogous iron(II) complexes and an aryl azide.

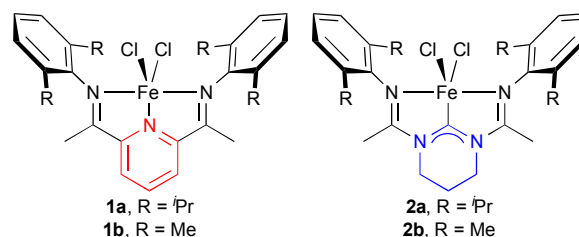


Figure 1. pyridyl diimine (**1**) and carbenodiamidine (**2**) complexes of iron.

Previously, we reported the synthesis of (CDA^{iPr})FeCl₂ (**2a**).¹¹ A high spin iron(II) configuration was assigned to the complex based on the solution magnetic moment (μ_{eff}) of 5.0 μ_{B} ($\chi \cdot T = 3.1 \text{ cm}^3 \cdot \text{K/mol}$) in THF and 4.6 μ_{B} ($\chi \cdot T = 2.7 \text{ cm}^3 \cdot \text{K/mol}$) in CH₂Cl₂ at 25 °C using Evans' method.¹⁶ One electron oxidation of **2a** was possible using acetylferrocenium tetrafluoroborate in CH₂Cl₂ to form [(CDA^{iPr})FeCl₂]BF₄ (**3**). The magnetic moment of 5.0 μ_{B} ($\chi \cdot T = 3.1 \text{ cm}^3 \cdot \text{K/mol}$) in THF at 25 °C is too low for a high spin iron(III) complex and too high for an intermediate spin iron(III) complex.

To further investigate the magnetic properties of **2a** and **3**, solid-state dc-magnetic susceptibility data were obtained from 2 K to 300 K (Figure 2). The samples demonstrated complex magnetic behaviour as a function of temperature. At low temperatures, both complexes had low magnetic moments that increased rapidly to a plateau at intermediate temperatures. Upon further heating, the magnetic moments underwent a gradual increase until the samples reached the maximum temperature achievable by the instrument.

The low magnetic moments observed at low temperatures for both **2a** and **3** are consistent with contributions from zero-field splitting, which is common for iron(II) and iron(III) complexes.¹⁷ The plateau in $\chi \cdot T$ for **2a** occurred from 30 K to 150 K and at 1.00

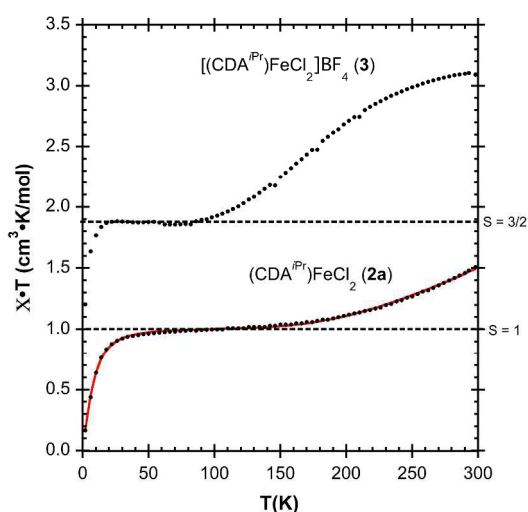


Figure 2. Variable temperature solid-state dc-magnetization data for **2a** and **3** using SQUID magnetometry. Filled symbols represent experimental data, and the solid line for **2a** represents the simulation obtained by combining two models: below 100 K, the data were fit to intermediate spin iron complexes with significant contributions from zero-field splitting (for $S = 1$ in **2a**: $g_{iso} = 2.01$, $|D| = 26 \text{ cm}^{-1}$, $|E| = 6 \text{ cm}^{-1}$; for $S = 3/2$ in **3** (fit shown in ESI): $g_{iso} = 2.01$, $|D| = 3.4 \text{ cm}^{-1}$, $|E| = 2.0 \text{ cm}^{-1}$) and above 100 K, the data were fit using $x = 1/[1 + \exp\{(\Delta H/R)(1/T - 1/T_c)\}]$ ($T_c = 563 \text{ K}$; $\Delta H = 705 \text{ cm}^{-1}$).¹⁷

$\text{cm}^3 \cdot \text{K/mol}$ is the same as the spin only value expected for an $S = 1$ metal complex. Above 150 K, the increase in magnetic moment suggests a spin state change from an $S = 1$ to an $S = 2$ ground state. These data could be fit using the Sorai domain model for spin equilibrium¹⁷ with a spin transition temperature (T_c) of 563 K that accounts for the incomplete transition that is observed by 300 K.¹⁸

A similar trend was observed for complex **3**, except the magnetic moment was found to be universally higher and evidence for a spin transition occurred at lower temperatures compared to **2a**. The plateau in $\chi \cdot T$ emerged at 25 K and persisted up to 100 K, and at $1.88 \text{ cm}^3 \cdot \text{K/mol}$ is consistent with the value for an $S = 3/2$ spin state. When the high temperature data ($>100 \text{ K}$) was modelled with the Sorai domain model, the best fit was a spin state change at 199 K from an $S = 3/2$ state to a higher spin state characterized by $\chi \cdot T = 3.13 \text{ cm}^3 \cdot \text{K/mol}$ (Figure S1). This value is significantly lower than the spin only value expected for a high spin $S = 5/2$ iron(III) centre ($4.39 \text{ cm}^3 \cdot \text{K/mol}$), which suggests that a spin equilibrium model may be inappropriate. As such, the fit was not included in Figure 2. Attempts to provide some clarity were made by evaluating **3** by EPR spectroscopy. However, solid state spectra collected at 10 K were complicated and suggested the presence of multiple $S = 3/2$ species (Figure S2).

To gain further insight, **2a** and **3** were analysed by variable temperature zero-field ^{57}Fe Mössbauer spectroscopy (Figures 3 and S2). At 90 K, the Mössbauer spectrum of $(\text{CDA}^{\text{Pr}})\text{FeCl}_2$ (**2a**) features an isomer shift of 0.31 mm/s and a quadrupole splitting of 2.14 mm/s (Figure 3). These values are consistent with an intermediate spin ($S = 1$) iron(II) centre as suggested by the SQUID measurements. Also consistent with the SQUID measurements were minimal changes in the Mössbauer spectrum between 100 and 150 K and significant changes upon warming to 295 K. The latter were characterized by a noticeable increase in the isomer shift ($\delta = 0.41 \text{ mm/s}$) and a slight decrease in the quadrupole splitting ($|\Delta E_Q| = 1.93 \text{ mm/s}$). Although the changes observed in the Mössbauer spectrum are consistent with a change in spin state, the observation of one rather

than two quadrupole doublets suggests either rapid interconversion between spin states¹⁹ or a quantum admixed $S = 1,2$ spin state at elevated temperatures.²⁰ We currently favour the former explanation because the latter has little precedence in ferrous compounds,²¹ and the SQUID data could be fit using a spin equilibrium model with magnetic moments for high and intermediate spin states that are within the range expected for $S = 1$ and $S = 2$ spin states (Figure 2).

Similar to **2a**, the Mössbauer spectrum of $[(\text{CDA}^{\text{Pr}})\text{FeCl}_2]\text{BF}_4$ (**3**) demonstrated isomer shifts at 100 K that were more consistent with an intermediate spin $S = 3/2$ iron(III) species ($\delta = 0.18 \text{ mm/s}$) than a high spin $S = 5/2$ complex (Figure S2). As the temperature was raised, a single quadrupole doublet was observed and a steady reduction in the quadrupole splitting from 2.21 mm/s to 1.62 mm/s occurred. As was the case with $(\text{CDA}^{\text{Pr}})\text{FeCl}_2$ (**2a**), the presence of one quadrupole doublet is atypical for conventional spin equilibrium behaviour and may be better explained by an $S = 3/2, 5/2$ quantum admixture.¹⁹ Quantum admixed $S = 3/2, 5/2$ spin states have precedence in iron porphyrin complexes²² and are believed to be important in many biological systems,²³ but examples such as this one that does not involve porphyrin ligands are uncommon.²⁴ The existence of an admixed spin state in **3** is further supported by the high temperature SQUID data, which begin to saturate towards magnetic moments that were too low for a pure $S = 5/2$ spin state.

As a final experiment directed towards understanding the spin transitions that appear to occur in these complexes, variable temperature X-ray crystallographic experiments were carried out.²⁵ Consistent with a change in spin state were considerable changes in metal-ligand bond distances in **2a** and **3** upon increasing the temperature (Table 1 and ESI for more temperatures). For example, the iron–carbene bond length in **2a** elongated from the abnormally short $1.812(2) \text{ \AA}$ to $1.882(3) \text{ \AA}$ and the average iron–amidine bond distances extended from $2.026(4) \text{ \AA}$ to $2.104(4) \text{ \AA}$ at 100 K and 250 K, respectively. Increases in bond length on the order of $0.07\text{--}0.08 \text{ \AA}$ are common for complexes of iron that undergo spin transitions.²⁶

To corroborate our experimental results, we carried out unrestricted DFT calculations on both **2a** and **3**. Intermediate ($S = 1$ and $3/2$) and high spin ($S = 2$ and $5/2$) configurations were calculated to be close in energy (*ca.* 5 kcal/mol) for both **2a** and **3**, but a low spin state configuration ($S = 1/2$) considered for **3** was significantly higher in energy ($> 15 \text{ kcal/mol}$). These findings are consistent with the small enthalpies (ΔH) obtained from fitting the SQUID data for

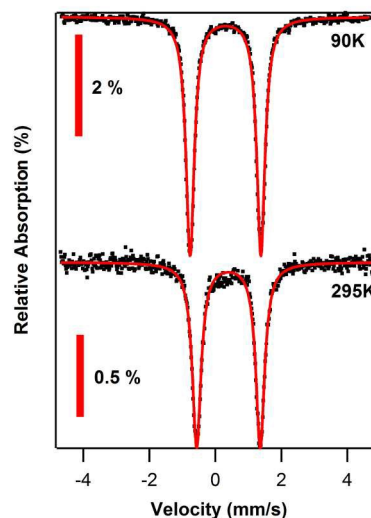


Figure 3. Zero-field ^{57}Fe Mössbauer spectra of **2a**. Simulation yields the following parameters: δ , $|\Delta E_Q|$ (mm/s) at 90 K: 0.31 , 2.14 ($\Gamma = 0.15 \text{ mm/s}$); at 295 K: 0.40 , 1.93 ($\Gamma = 0.16 \text{ mm/s}$) where $\Gamma =$ half width at half height.

Table 1. Selected bond lengths (Å) and Mössbauer parameters ($^{\text{mm}}/\text{s}$) for **2a** and **3**. See ESI for additional bond lengths and temperatures.

	(CDA ^{IPr})FeCl ₂ (2a)				[(CDA ^{IPr})FeCl ₂]BF ₄ (3)			
	Exp.		Calc.		Exp.		Calc.	
	100 K	250 K	S = 1	S = 2	80 K	298 K	S = ³ / ₂	S = ⁵ / ₂
Fe–carbene	1.812(2)	1.882(3)	1.823	2.024	1.908(2)	2.033(2)	1.904	2.105
Fe–amidine ^a	2.026(4)	2.104(4)	2.071	2.284	2.031(9)	2.142(12)	2.102	2.262
δ	0.31 ^b	0.40 ^c	0.42	0.70	0.18 ^d	0.21	0.32	0.33
ΔE ₀	2.14 ^b	1.93 ^c	2.17	1.43	2.21 ^d	1.58	2.78	1.67

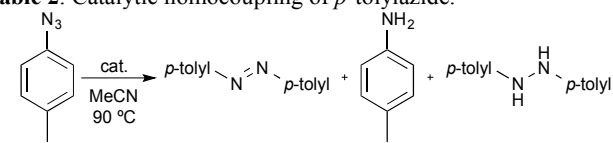
^aReported as an average. ^bMeasured at 90 K. ^cMeasured at 295 K. ^dMeasured at 100 K.

2a and also with a spin admix situation in **3** (Figure 2). Moreover, comparing calculated and experimental metal–ligand bond lengths supports intermediate spin state assignments for **2a** and **3** at low temperatures (<100 K). At elevated temperatures (>100 K), the experimental bond lengths move towards what is calculated for a high spin state structure (Table 1). Also consistent with this assignment were the Mössbauer parameters, which were calculated to be close to the experimental values observed at low temperature for the intermediate spin state electronic configuration (Table 1). Calculations for the Mössbauer parameters in **3** were not as definitive as **2a** for distinguishing intermediate and high spin configurations because the predicted isomer shifts were virtually identical for both electronic configurations. However, the quadrupole splitting was predicted to decrease with the spin transition, which is consistent with the experimental data (Table 1).

Based on our magnetic, spectroscopic, crystallographic, and computational investigations, we hypothesized that the electronic features of the complexes were due to the σ-donating capabilities of the CDA ligands, which served to increase ligand field splitting and stabilize intermediate spin states. We reasoned that these capabilities could be beneficial for reactions between azides and alkenes, which may proceed through high oxidation state intermediates that could benefit from being stabilized by σ-donating ligands. Therefore, we undertook an investigation into the reactivity of **2a** with aryl azides in the presence of 1-octene. Unfortunately, reactions catalysed by **1a** or **2a** at 50 °C demonstrated no conversion of either starting material (Table S1). At higher temperatures, aziridines were observed with both precatalysts, but the quantity was not significantly above the background reaction. A by-product in reactions using **2a** at 90 °C was the homodimerization of azides to form diazenes, which did not occur in the absence of the iron catalyst (Table 2, entry 1).

To demonstrate the importance of the supporting ligand for the aryl azide homocoupling reaction, a comparison was made between (PDI^{IPr})FeCl₂ (**1a**), (CDA^{IPr})FeCl₂ (**2a**), and FeCl₂ as catalysts (Table 2). After 14 hours, FeCl₂, (PDI^{IPr})FeCl₂ (**1a**), and (CDA^{IPr})FeCl₂ (**2a**) demonstrated significantly different reactivity resulting in 32%, 78%, and 86% conversion of *p*-tolylazide, respectively. Whereas reactions with FeCl₂ produced *p*-toluidine as the major product (entry 2), reactions catalysed by **1a** and **2a** gave diazene as the major product with *p*-toluidine being the only by-product (entries 3 and 4). Envisioning a mechanism where a high oxidation state iron-nitrene intermediate interacts with an equivalent of azide to liberate the diazene product,²⁷ we surmised that a decrease in steric bulk around the iron centre would lead to a more efficient reaction. Consistent with this hypothesis were reactions carried out with the less sterically encumbered (PDI^{Me})FeCl₂ (**1b**, entry 5) and (CDA^{Me})FeCl₂ (**2b**, entry 6), which both proceeded with 91% conversion and greater formation of the diazene product (6:1 and 10:1 selectivity). Kinetic measurements revealed that the rate of azide conversion for **2b** was nearly five times faster than for **1b** and **2a**, and over an order of magnitude faster than for FeCl₂ (Table 2).

An alternative mechanism that may be operative is the iron-catalysed decomposition of aryl azide to form free triplet nitrene, which then undergoes rapid dimerization to form a diazene.²⁸ Two pieces of experimental evidence are inconsistent with this mechanism. Firstly, *p*-tolylazide was irradiated with UV light and subjected to the reaction conditions. Since this procedure produces free triplet nitrene,²⁹ we reasoned that the product distribution would be similar to the iron-catalysed processes if both reactions proceed through a common triplet nitrene intermediate. During photolysis, diazene (54%) was observed as the major product, but unlike the iron-catalysed processes, no *p*-toluidine was produced and hydrazine (28%) was observed as an additional product (Table 2, entry 7). These data suggest that the photolysis and iron-catalysed processes do not proceed through a common intermediate. Further contradicting a mechanism involving a free nitrene were differences in reactivity observed for reactions between *p*-tolylazide and 1-octene at 50 °C (Table S1). Unlike reactions catalysed by **1a**, **1b**, or **2a**, reactions catalysed by **2b** resulted in the formation of aziridine as the major product (28%) with diazene being formed as a minor by-product (5%). Once again, reactions carried out under photolysis demonstrated a different product distribution leading to diazene as the major product (25%) with aziridine being formed as a minor by-product (10%). Unfortunately, the formation of significant quantities of other unidentified by-products precluded the use of **2b** as catalysts for the aziridination of olefins. Nevertheless, the reactivity of **2b** compared to **1b** demonstrates the potential benefit of iron complexes supported by CDA ligands.

Table 2. Catalytic homocoupling of *p*-tolylazide.


entry	cat.	selectivity ^a	k _{obs} (× 10 ⁻⁵ s ⁻¹)
1	none	0 ^b	0 ^b
2	FeCl ₂	1:2:0	0.906
3	(PDI ^{IPr})FeCl ₂ (1a)	3:1:0	4.18
4	(CDA ^{IPr})FeCl ₂ (2a)	4:1:0	5.18
5	(PDI ^{Me})FeCl ₂ (1b)	6:1:0	4.51
6	(CDA ^{Me})FeCl ₂ (2b)	10:1:0	20.2
7	hv ^c	2:0:1	3.09

^aSelectivity = diazene/*p*-toluidine/hydrazine. ^bConv. = 0%.

Considering the renewed interest in base metals for chemical catalysis and the usefulness that N-heterocyclic carbene ligands have demonstrated for organotransition metal catalysis, the investigations presented above have provided insight into the electronic consequences that may result by ligating NHC ligands to iron. Furthermore, a comparison of the CDA ligands to analogous PDI complexes highlight the importance of the electron donating capabilities of the central neutral donor in this class of pincer-type

ligands. Although promiscuous reactivity have precluded the use of **2b** in aziridination reactions, the differences observed between **2b** and catalysts containing PDI ligands is encouraging for the development of unique catalytic reactions that bear CDA ligands. Our future efforts will be directed towards discovering such reactions by applying these complexes as catalysts for a variety of reactions involving multiple oxidation states of iron. The results from these investigations will be forthcoming.

The authors thank Prof. Theodore Betley, Dr. Shaoyan Chu, Prof. T. David Harris, Prof. Bart M. Bartlett, Stephanie Daifuku, and Prof. Michael Neidig for assistance with Mössbauer, SQUID, and EPR measurements. The authors are also grateful to Prof. Paul Chirik and Dr. Chantal Stieber for computational assistance. Acknowledgment is made to the donors of the American Chemical Society Petroleum Research Fund (PRF# 53621-DNI3) for support of this research.

Notes and references

^a This paper is dedicated in memoriam to Gregory L. Hillhouse.

^b Eugene F. Merkert Chemistry Center, Department of Chemistry, Boston College, 2609 Beacon Street, Chestnut Hill, Massachusetts, 02467.

^c Department of Chemistry and Chemical Biology, Harvard University, 12 Oxford Street, Cambridge, Massachusetts, 02138.

† Electronic Supplementary Information (ESI) available: CIF files for complex **2a** (CCDC 900881, 927786 – 927788) and **3** (CCDC 927790 - 927794), general considerations, computational methods, synthetic procedures and characterization for all new complexes. See DOI: 10.1039/c000000x/

- B. L. Small, M. Brookhart and A. M. A. Bennett, *J. Am. Chem. Soc.* 1998, **120**, 4049.
- (a) G. J. P. Britovsek, V. C. Gibson, B. S. Kimberley, P. J. Maddox, S. J. McTavish, G. A. Sloan, A. J. P. White and D. J. Williams, *Chem. Commun.* 1998, 849; (b) G. J. P. Britovsek, M. Bruce, V. C. Gibson, B. S. Kimberley, P. J. Maddox, S. Mastroianni, S. J. McTavish, C. Redshaw, G. A. Sloan, S. Strömberg, A. J. P. White and D. J. Williams, *J. Am. Chem. Soc.* 1999, **121**, 8728.
- (a) B. L. Small and M. Brookhart, *J. Am. Chem. Soc.* 1998, **120**, 7143; (b) C. Bianchini, G. Giambastiani, I. G. Rios, G. Mantovani, A. Meli and A. M. Segarra, *Coord. Chem. Rev.* 2006, **250**, 1391.
- S. S. Karpiniec, D. S. McGuinness, G. J. P. Britovsek and J. Patel, *Organometallics* 2012, **31**, 3439.
- R. K. O'Reilly, V. C. Gibson, A. J. P. White and D. J. Williams, *Polyhedron* 2004, **23**, 2921.
- A. B. Biernesser, B. Li and J. A. Byers, *J. Am. Chem. Soc.* 2013, **135**, 16553.
- (a) S. C. Bart, E. Lobkovsky and P. J. Chirik, *J. Am. Chem. Soc.* 2004, **126**, 13794; (b) R. J. Trovitch, E. Lobkovsky, E. Bill and P. J. Chirik, *Organometallics* 2008, **27**, 1470; (c) S. Monfette, Z. R. Turner, S. P. Semproni and P. J. Chirik, *J. Am. Chem. Soc.* 2012, **134**, 4561.
- A. M. Tondreau, C. C. H. Atienza, K. J. Weller, S. A. Nye, K. M. Lewis, J. G. P. Delis and P. J. Chirik, *Science* 2012, **335**, 567.
- J. V. Obligacion and P. J. Chirik, *J. Am. Chem. Soc.* 2013, **135**, 19107.
- (a) M. W. Bouwkamp, A. C. Bowman, E. Lobkovsky and P. J. Chirik, *J. Am. Chem. Soc.* 2006, **128**, 13340; (b) S. K. Russel, E. Lobkovsky and P. J. Chirik, *J. Am. Chem. Soc.* 2011, **133**, 8858.
- H. Z. Kaplan, B. Li and J. A. Byers, *Organometallics* 2012, **31**, 7343.
- A similar complex was reported almost simultaneously, but the structure was not confirmed crystallographically: J. A. Thagfi and G. G. Lavoie, *Organometallics* 2012, **31**, 7351.
- (a) M. Iglesias, D. J. Beetstra, J. C. Knight, L.-L. Ooi, A. Stasch, S. Coles, L. Male, M. B. Hursthouse, K. J. Cavell, A. Dervisi and I. A. Fallis, *Organometallics* 2008, **27**, 3279; (b) V. Friese, S. Nag, J. Wang, M.-P. Santoni, A. Rodrigue-Witchel, G. S. Hanan and F. Schaper, *Eur. J. Inorg. Chem.* 2011, 39.
- Other short iron–NHC bonds: (a) B. Liu, Q. Xia and W. Chen, *Angew. Chem. Int. Ed.* 2009, **48**, 5513; (b) Y. Ohki, T. Hatanaka and K. Tatsumi, *J. Am. Chem. Soc.* 2008, **130**, 17174.
- C. M. Manna, H. Z. Kaplan, B. Li and J. A. Byers, *Polyhedron* 2014, **84**, 160.
- (a) D. F. Evans, *J. Chem. Soc.* 1959, 2003–2005; (b) E. M. Schubert, *J. Chem. Educ.* 1992, **69**, 62.
- O. Kahn, *Molecular Magnetism*, VCH Publishers, Inc.: New York, N. Y., 1993.
- Solution and solid state magnetic moments for **2a** differed, which likely reflects a different distribution of spin states in the solid and solution state. Solvent dependent magnetic moments are consistent with this hypothesis, which coincidentally results in identical magnetic moments for **2a** and **3**.
- (a) R. Rickards, C. E. Johnso, and H. A. O. Hill *J. Chem. Phys.* 1968, **48**, 5231. (b) O. Hiroki, M. Yonezo, and T. Yoshimasa *Inorg. Chem.* **22**, 2684.
- Quantum admixed spin states are characterized by only one set of Mössbauer quadrupole doublets and a decrease in quadrupole splitting (ΔE_Q) as the temperature is increased. (a) M. M. Maltempo, *J. Chem. Phys.* 1974, **61**, 2540; (b) H. D. Dolphin, J. R. Sams and T. B. Tsin, *Inorg. Chem.* 1977, **16**, 711.
- X.-Y. Kuang, and K.-W. Zhou *J. Phys. Chem. A* 2005, **109**, 10129.
- Nakamura, *M. Coord. Chem. Rev.* 2006, **250**, 2271.
- R. Weiss, A. Gold, and J. Turner *Chem. Rev.* 2006, **106**, 2550.
- (a) M. D. Fryzuk, D. B. Leznoff, E. S. F. Ma, S. J. Rettig, and V. G. Young Jr. *Organometallics* 1998, **17**, 2313. (b) G. Mund, R. J. Batchelor, R. D. Sharma, C. H. W. Jones, D. B. Leznoff *J. Chem. Soc., Dalton Trans.* 2002, 136. (c) P. J. Alonso, A. B. Arauzo, J. Fornies, M. A. Garcia-Monforte, A. Martin, J. I. Martinez, C. Rillo, and J. J. Saiz-Garitaonandia *Angewandte Chem. Int. Ed.* 2006, **188**, 6859.
- S. Mossin, B. L. Tran, D. Adhikari, M. Pink, F. W. Heinemann, J. Sutter, R. K. Szilagyi, K. Meyer and D. J. Mendiola, *J. Am. Chem. Soc.* 2012, **134**, 13651.
- (a) W. Broeckx, N. Overbergh, C. Samyn, G. Smets and G. L'Abbé, *Tetrahedron*, 1971, **27**, 3527; (b) C.-K. Sha, S.-L. Ouyang, D.-Y. Hsieh, R.-C. Chang and S.-C. Chang, *J. Org. Chem.* 1986, **51**, 1490.
- K. Riener, S. Haslinger, A. Raba, M. O. Högerl, M. Kokoja, W. A. Herrmann and F. E. Kühn, *Chem. Rev.* 2014, **114**, 5215.
- (a) M. M. Abu-Omar, C. E. Shields, N. Y. Edwards, and R. A. Eikley *Angew. Chem. Int. Ed.* 2005, **44**, 6203; (b) A. Takaoka, M.-E. Moret, and J. C. Peters *J. Am. Chem. Soc.* 2011, **134**, 6695. (c) W. H. Harman, M. F. Lichterma, N. A. Piro, and C. J. Chang *Inorganic Chemistry* 2012, **51**, 10037.
- A. Reiser, F. W. Willets, G. C. Terry, V. Williams, and R. Marley *Trans. Faraday Soc.* 1968, **64**, 3265.